

## High-Resolution Electron Microscopy Study of Hafnium Nitride Chloride

Judith Oró-Solé,<sup>†</sup> Maria Teresa Caldes,<sup>‡</sup>  
M. Rosa Palacín,<sup>†</sup> Mikhail Vlassov,<sup>†,§</sup>  
Daniel Beltrán-Porter,<sup>‡</sup> and Amparo Fuertes\*,<sup>†</sup>

*Institut de Ciència de Materials de Barcelona (C.S.I.C.), Campus U.A.B., 08193 Bellaterra, Spain; Institut de Ciència de Materials de la Universitat de València, P.O. Box 2085, 46071 Burjassot, Spain; and Institut de Matériaux Jean Rouxel UMR 6502, 2, rue de la Houssinière, 44072 Nantes CEDEX 03, France*

Received August 4, 1999

Metal- or metallocene-intercalated hafnium and zirconium nitride halides of formula  $A_xMNX$  ( $A$  = alkaline metal;  $M$  = Zr and Hf;  $X$  = Cl, Br) constitute a new class of superconducting compounds raising critical temperatures up to 25 K.<sup>1–6</sup> The space group and the crystal structure of the host lattices  $\beta$ -MNX have been recently determined by electron diffraction and Rietveld refinement of X-ray and neutron powder diffraction data.<sup>3–5</sup> This structure can be considered as resulting from the intercalation of N atoms in all of the tetrahedral interstices inside the double-metal layers of the zirconium monochloride structure, preserving the space group  $R\bar{3}m$  with similar crystal parameters.<sup>7,8</sup> The structure of ZrCl consists of cubic-close packed layers of metal and halide atoms stacked in pairs yielding the sequence Cl–Zr–Zr–Cl (Figure 1a). Besides the above-mentioned nitride compound, there are several examples of intercalation derivatives of ZrCl with different anions occupying tetrahedral interstices such as  $O^{2-}$  in  $ZrClO_{0.5}$ <sup>9</sup> and  $H^-$  in  $Zr_2Cl_2H$ , but intercalation in octahedral sites is also possible and is exemplified by  $C^{4-}$  in  $Zr_2Cl_2C$ <sup>10</sup> or  $H_2$  in  $Zr_2Cl_2H_2$ .<sup>11</sup> Analogous bromide compounds isostructural with the respective chlorides<sup>12</sup> are known, and in many cases, the corresponding hafnium derivatives exist (although, as the parent HfCl, they frequently show the packing sequence of the ZrBr structure<sup>13</sup>). In recent papers, we have reported the

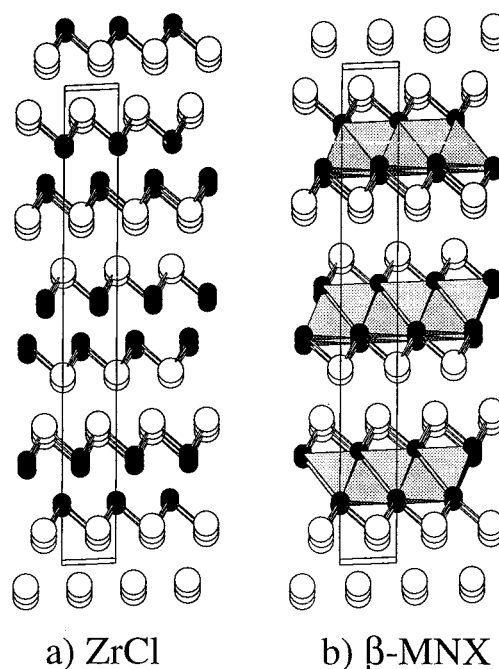


**Figure 1.** Crystal structures of (a) ZrCl<sup>7</sup> and (b) host lattice for the superconductors  $Li_xMNX$  ( $M$  = Zr, Hf;  $X$  = Cl, Br).<sup>3</sup> Black and white spheres represent metal and halide atoms, respectively. Nitrogen atoms are placed at the center of the tetrahedra.

crystal structure determination of three isostructural  $\beta$ -MNX compounds ( $M$  = Zr, Hf;  $X$  = Cl, Br),<sup>3</sup> (see Figure 1b) and the comparison of the synthesis and intercalation chemistry of the superconductors  $Li_xZrNCl$ ,  $Li_xHfNCl$ , and  $Li_xZrNBr$ .<sup>14</sup> We described that the chemical or electrochemical lithium intercalation behavior of  $\beta$ -HfNCl is strongly dependent on the chemical history of each sample, whereas this is not the case for the zirconium derivatives ( $\beta$ -ZrNBr and  $\beta$ -ZrNCl). Different batches of  $\beta$ -HfNCl with impurity-free powder X-ray diffraction patterns were subjected to the same treatment in *n*-butyllithium. The resulting lithium uptakes ranged from 0.07 to 0.67 mol per formula, leading to either nonsuperconducting compounds or superconducting ones with critical temperatures up to 24 K.<sup>14</sup> We have also already reported that the electrochemical capacity on discharge of  $\beta$ -MNX compounds is affected by the milling step in the process of electrode preparation, with strong grinding resulting in a drastic diminution of the lithium intercalation degree. In this paper, we show the first high-resolution electron microscopy study of  $\beta$ -HfNCl. The results of this study, performed on different batches, indicate that the intercalation capacity of the hafnium compound is strongly hindered by the presence of oxygen impurities in the sample. Independently, the grinding of the samples is shown to induce displacement of the layers along the *c* direction, thus preventing the diffusion of lithium into the van der Waals gap and hence the induction of superconductivity.

(14) Vlassov, M.; Palacín, M. R.; Beltrán-Porter, D.; Oró-Solé, J.; Canadell, E.; Alemany, P.; Fuertes, A. *Inorg. Chem.* **1999**, *38*, 4530.

<sup>†</sup> C.S.I.C.

<sup>‡</sup> Institut de Ciència de Materials de la Universitat de València.

<sup>§</sup> Permanent address: Earthcrust Research Institute, St. Petersburg University, Russia.

<sup>||</sup> Institut de Matériaux Jean Rouxel UMR.

(1) Yamanaka, S.; Hohetama, K.; Kawaji, H. *Nature* **1998**, *392*, 580.

(2) (a) Yamanaka, S.; Kawaji, H.; Hotehama, K.; Ohashi, M. *Adv. Mater.* **1996**, *8*, 771. (b) Kawaji, H.; Hotehama, K.; Yamanaka, S. *Chem. Mat.* **1997**, *9*, 2127.

(3) Fuertes, A.; Vlassov, M.; Beltrán-Porter, D.; Alemany, P.; Canadell, E.; Casañ-Pastor, N.; Palacín, M. R. *Chem. Mater.* **1999**, *11*, 203.

(4) Fogg, A. M.; Evans, S. O.; O'Hare, D. *Chem. Commun.* **1998**, 2269.

(5) Shamoto, S.; Kato, T.; Ono, Y.; Miyazaki, Y.; Ohoyama, K.; Ohashi, M.; Yamaguchi, Y.; Kajitani, T. *Physica C* **1998**, *306*, 7.

(6) Fogg, A. M.; Green, V. M.; O'Hare, D. *Chem. Mater.* **1999**, *11*, 216.

(7) Adolphson, D. G.; Corbett, J. D. *Inorg. Chem.* **1976**, *15*, 1820.

(8) Ford, J. E.; Corbett, J. D.; Hwu, S. *Inorg. Chem.* **1983**, *22*, 2789 and references therein.

(9) Seaverson, L. M.; Corbett, J. D. *Inorg. Chem.* **1983**, *22*, 3202.

(10) Ford, J.; Corbett, J. D.; Hwu, S. *Inorg. Chem.* **1983**, *22*, 2790.

(11) Struss, A. W.; Corbett, J. D. *Inorg. Chem.* **1977**, *16*, 360.

(12) Wijeyesekera, S. D.; Corbett, J. D. *Inorg. Chem.* **1986**, *25*, 4709.

(13) Daake, R. L.; Corbett, J. D. *Inorg. Chem.* **1977**, *16*, 2029.

Samples of  $\beta$ -HfNCl were prepared in evacuated quartz tubes by the reaction of Hf (Aldrich 99.5%) with  $\text{NH}_4\text{Cl}$  (Aldrich, 99.9%) at 850 °C, followed by recrystallization via vapor transport under conditions previously reported.<sup>15</sup> Elemental analysis was performed to determine N and H contents. Chemical lithiation reactions were done at 50 °C by dispersion of the powders in a 0.1 M solution of *n*-butyllithium in hexane (Aldrich) for 140 h, using Ar-filled, sealed glass tubes. The resulting lithium contents were determined by atomic emission analysis. Electrochemical tests were made on powder samples with Swagelok two-electrode cells using lithium foil as counter electrode and 1 M  $\text{LiPF}_6$  in 1:1 EC/DMC (ethylene carbonate/dimethyl carbonate) as electrolyte. Handling of lithiated samples and cell preparation were done in an Ar-filled glovebox. Samples for transmission electron microscopy were prepared by dispersing the powder in *n*-heptane and depositing the solution on a holey carbon aluminum grid. Electron diffraction patterns and XEDS analyses were obtained in Hitachi H9000NAR and Philips CM30 electron microscopes operating at 300 kV. The Scherzer resolutions were 1.8 and 2.5 Å for the Hitachi and the Philips instruments, respectively. Calculated images for different defocus and different thicknesses were obtained using the Mactempas program.

A typical experimental HREM image along [010] of a  $\beta$ -HfNCl sample that intercalates 0.67 lithium atoms per formula unit is shown in Figure 2. This sample shows a superconducting behavior below 24 K and particle sizes lower than 1.5  $\mu\text{m}$  for 70% of the crystals.<sup>14</sup> On the other hand, its electrochemical capacity on discharge was consistent with the lithium uptake observed by chemical methods. The calculated images as functions of defocus and thickness based on the structural model from Fuertes et al.<sup>3</sup> are shown in Figure 3. The HREM image of Figure 2a is in relatively good agreement with the calculated image for a thickness of 90 Å and a defocus of 0 Å (see Figures 2-b and 3). To improve the observed contrast, especially in the thicker part of the crystal, the experimental image was processed. In the filtered image (Figure 2b), the intense bright dots correspond to the Hf double layer and the diffuse maxima to the chlorine configuration, respectively. The material is stable under the electron beam and shows a regular stacking of the Cl–Hf–N–N–Hf–Cl double layers, being almost free of defects from the inner part of the crystals to their thin edges. The observed *c* parameter (27.7 Å) is the same as that refined from X-ray powder diffraction data.<sup>3</sup>

A representative experimental HREM image along [010] of a sample intercalating 0.07 lithium atoms per formula is shown on Figure 4. The electrochemical capacity on discharge for this material is much lower than that for the preceding sample, and the corresponding lithiated compound did not show any superconducting transition down to 4 K.<sup>14</sup> Crystals generally showed two zones with different image contrasts, labeled A and B and corresponding to the edges and cores, respectively. These crystals were found to be unstable under

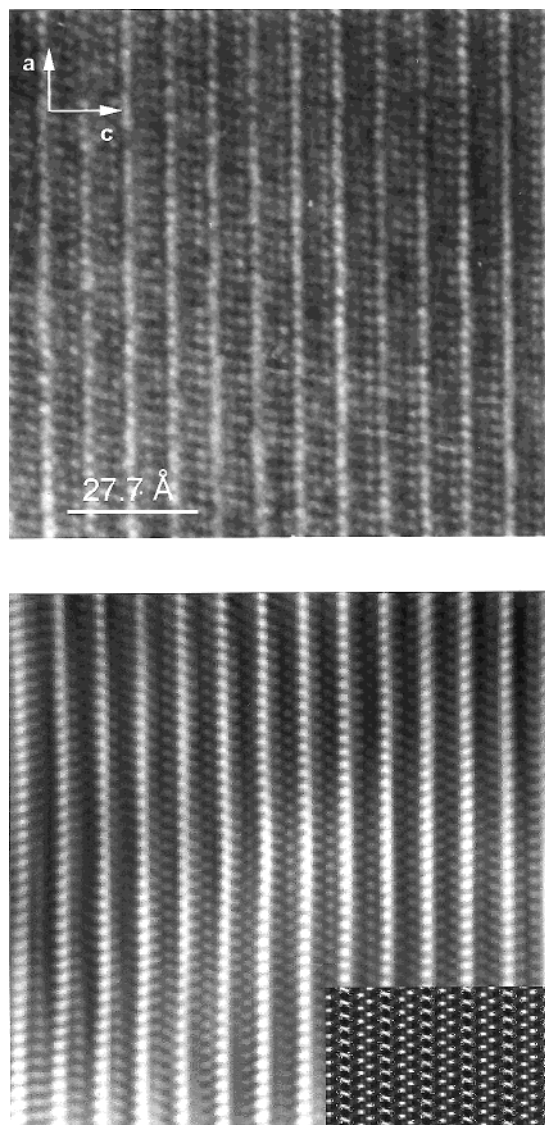


**Figure 2.** (a) Experimental HREM image of  $\beta$ -HfNCl along [010]. (b) Filtered image and (inset) computer overlay of the projected crystal structure and the computer-simulated image (thickness = 90 Å and defocus = 0 Å). The bright dots identify the Hf configuration.

the electron beam, with a long observation time leading to a growth of the A zone size. The XEDS analyses performed independently on both zones (Figure 4) showed the spectrum characteristic of composition "HfNCl" only in the B part.<sup>3</sup> The image contrast corresponding to this zone is similar to that shown in Figure 2, although some disorder is observed in the stacking of the layers along the *c* axis. In the XEDS spectrum of the A zone, the peaks characteristic of chlorine were not present and the presence of oxygen was clearly evident. In Figure 5, we show the HREM image of a different crystal of the same sample showing two A type zones with different orientations. The Fourier transforms corresponding to the experimental image of both orientations are depicted as insets on the same figure. The two dimensional (2D) symmetry of these patterns is monoclinic, and the observed *d* spacings of 3.12, 2.59, 5.07, and 3.67 Å may be assigned respectively to the  $d_{11\bar{1}}$ ,  $d_{020}$ ,  $d_{100}$ , and  $d_{01\bar{1}}$  spacings of  $\text{HfO}_2$ .<sup>16</sup> The zone axes for these planes are [011] and [101]. The observation of  $\text{HfO}_2$  in the thin edges of the crystals is typical for all

(15) Fuertes, A.; Vlassov, M.; Beltrán Porter, D.; Palacín Peiró, M. R. Procedimiento de obtención de nitruro-haluros de zirconio y hafnio mediante síntesis en reactor cerrado. Patent application Number 9901978, Oficina Española de patentes y marcas, Spain, 1999.

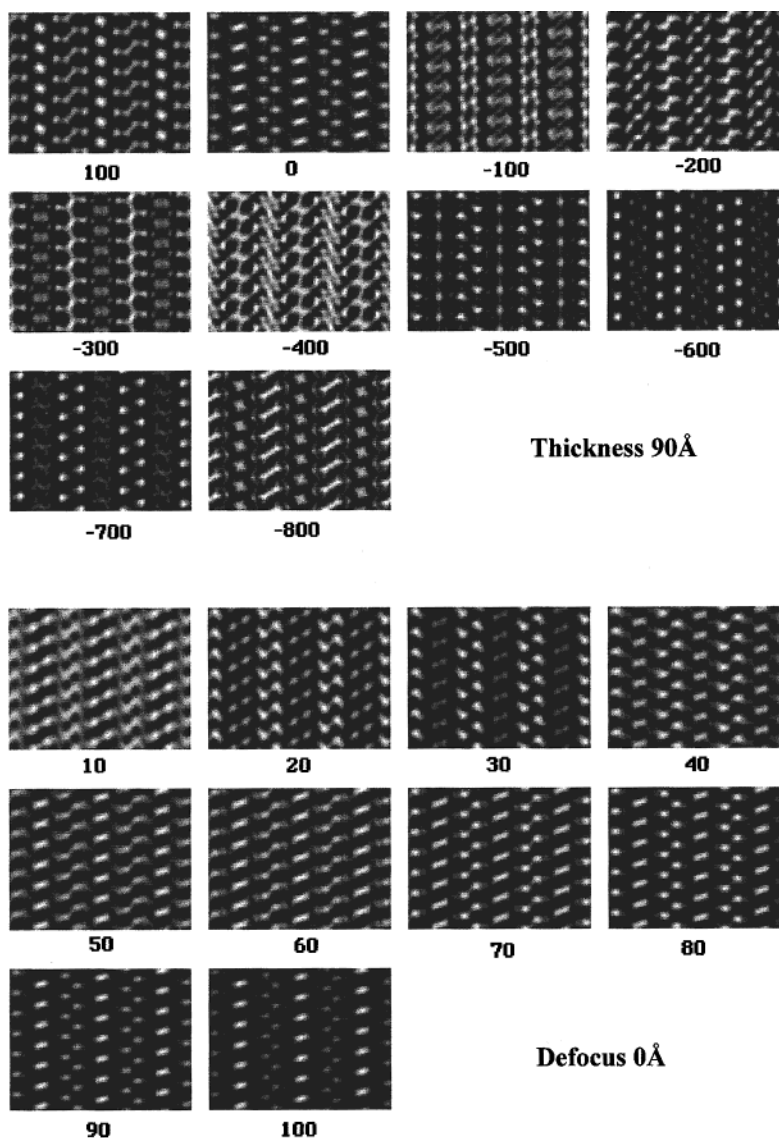


**Figure 3.** Computer-simulated HREM images of  $\beta$ -HfNCl as a function of defocus (in angstroms) (top) and thickness (in angstroms) (bottom).

samples showing a low lithium uptake. On the contrary, in samples with higher lithium intercalation degrees, the image contrast of Figure 2 is always uniformly observed throughout the whole crystal (see Figure 6 for a lower resolution image showing the edge of a crystal from such a sample). By taking into account the high vacuum conditions of the HREM experiments, the  $\text{HfO}_2$  film growing under the electron beam can only come as a decomposition product from crystals already containing oxygen impurities. These oxygen atoms would presumably occupy some of the tetrahedral interstices of the structure (as in  $\text{ZrClO}_y$ ), the real composition of the samples being  $\text{HfN}_x\text{O}_y\text{Cl}$ . As the  $\text{HfO}_2$  film is already observed at the very beginning of the electron microscopy study, we believe that it may also have started to form during the synthesis (i.e., in the transport purification step). In both cases, this oxygen should come from impurities in reactants, Hf or  $\text{NH}_4\text{Cl}$ . Indeed, the oxygen scavenger ability of Zr and Hf is well-established; for instance, Zr is able to dissolve oxygen up to a saturation limit of  $\text{ZrO}_{0.42}$ .<sup>17,18</sup> In agreement with these hypotheses,

we have clearly observed that the HfNCl samples exhibiting high lithium uptakes were obtained only in the cases where extreme precautions to avoid oxygen, in the reactants as well as in the reaction tube, were taken. As stated before, oxygen may occupy the tetrahedral interstices of the ZrCl structure to form  $\text{ZrClO}_y$  ( $y \leq 0.45$ ) that, contrasting with the chemical stability of ZrNCl, is moisture- and air-sensitive.<sup>9</sup> Although they have not been reported to date, the HfCl and HfNCl oxygen intercalation compounds ( $\text{HfClO}_y$ ,  $\text{HfClN}_x\text{O}_y$ ) may certainly exist. In the latter case, oxygen and nitrogen atoms would occupy the tetrahedral sites of the HfCl structure. The observed irreproducibility in the lithium uptake degree may be explained by taking into account several factors. On one hand, the existence of a layer of  $\text{HfO}_2$  in the surface of the crystals acts as a physical barrier preventing lithium intercalation. On the other hand, doping of  $\text{HfN}_x\text{O}_y\text{Cl}$  might be harder due to the fact that it is already doped. Indeed, the partial

(17) Miller, G. L. *Zirconium*; Butterworth Publications Limited: London, 1957.

(18) Ackerman, R. J.; Garg, S. P.; Rauh, E. G. *J. Am. Ceram. Soc.* **1977**, *60*, 341.

(16) Ruh, R.; Corfield, P. W. R. *J. Am. Ceram. Soc.* **1970**, *53*, 126.

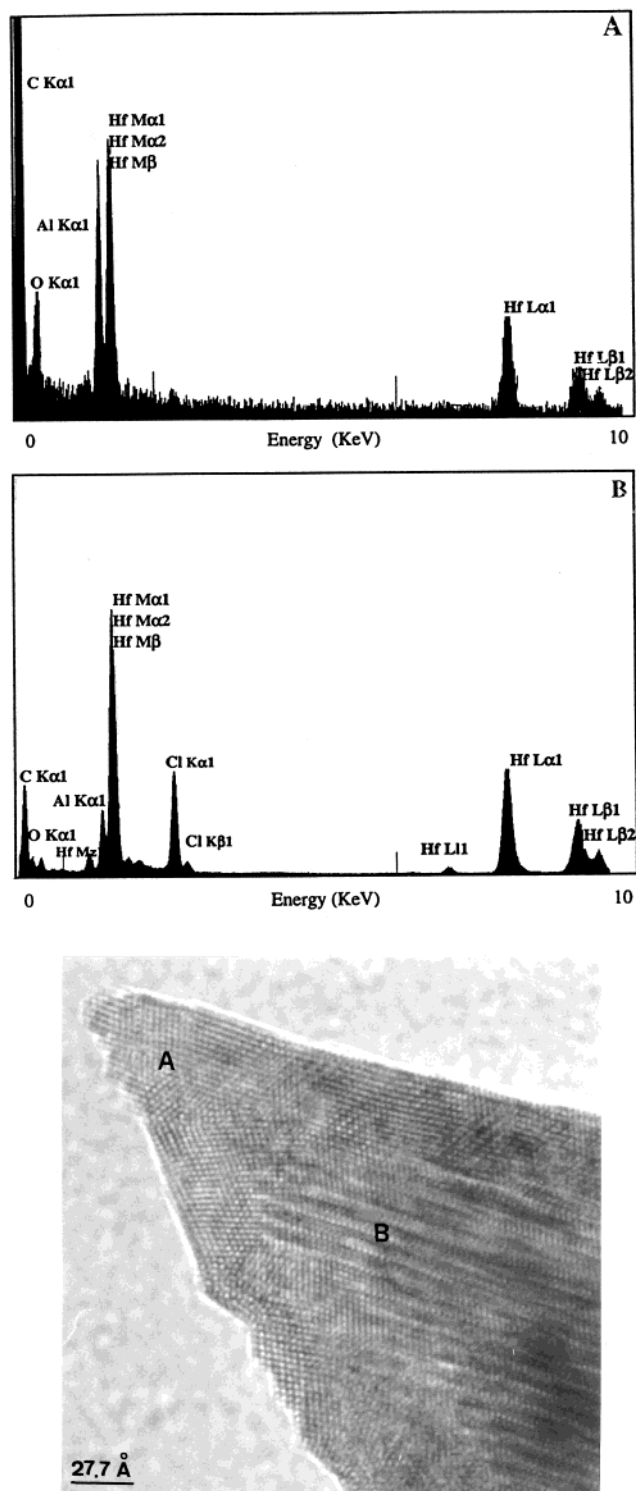


**Figure 4.** Experimental HREM image along [010] and XEDS analyses of a sample of  $\beta$ -HfNCl that intercalates 0.07 lithium atoms per formula. The two zones, A and B, correspond to domains of HfO<sub>2</sub> and  $\beta$ -HfNCl, respectively.

substitution of nitrogen (formal valence: -3) by oxygen (formal valence: -2) leads to electron doping, as does the introduction of lithium into the van der Waals gap.

Another factor generally known to obstruct lithium diffusion in layered structures is the existence of extended defects. In the case of  $\beta$ -HfNCl, these defects can be created in oxygen-free (i.e., with high lithium intercalation ability) samples by mechanical treatment, even by simply manual milling. Indeed, images taken

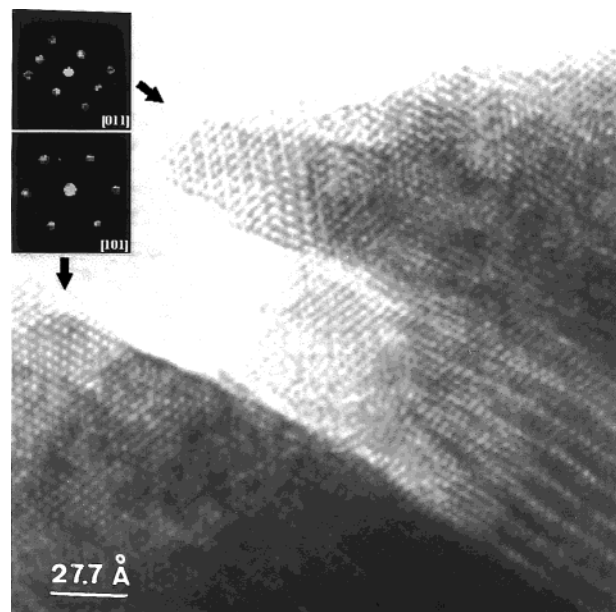


**Figure 5.** High-resolution electron microscopy image along [010] of a crystal showing two different orientations for HfO<sub>2</sub> zones. Insets: corresponding Fourier transforms.

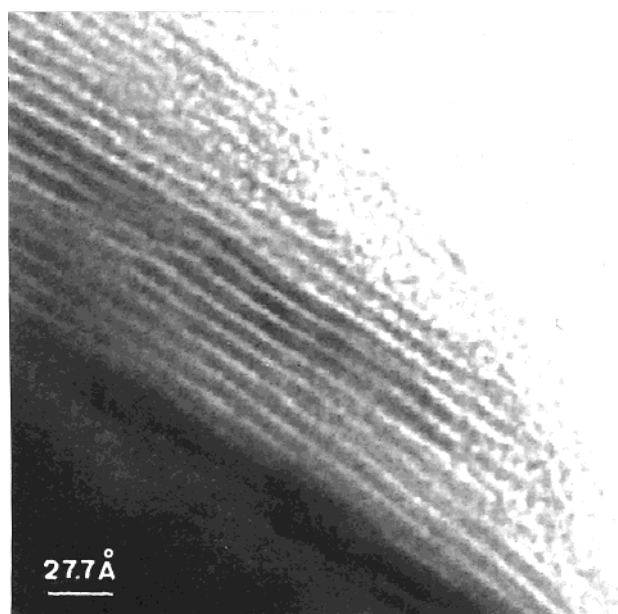


**Figure 6.** High-resolution electron microscopy image along [010] of a sample intercalating 0.67 lithium atoms per formula, showing the thin edge of the crystal.

on samples after manual grinding indicate that a displacement of the layers along a direction parallel to the *c* axis occurs (see Figure 7). As a result of these displacements, the van der Waals gaps are blocked, and hence, lithium diffusion is prevented. This fact explains our previous observation<sup>14</sup> that milling treatment drastically reduces the electrochemical capacity on discharge for  $\beta$ -HfNCl.

The HREM study described in this paper is currently being extended to  $\beta$ -ZrNCl and  $\beta$ -ZrNBr. Preliminary results show no MO<sub>2</sub> zones in the edges of crystals for these zirconium derivatives. This observation is in agreement with the reproducibility observed in the synthesis and intercalating behavior of these samples,<sup>14</sup> thus reinforcing the idea that oxygen contamination is

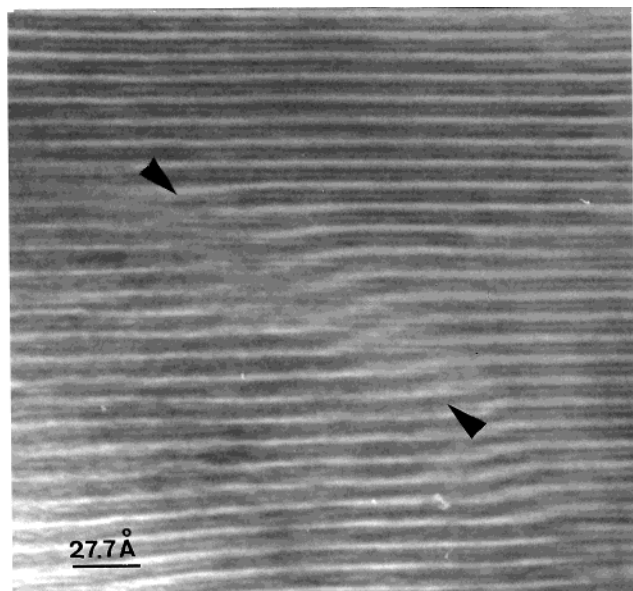


**Figure 7.** High-resolution electron microscopy image of a manually ground sample of  $\beta$ -HfNCl.

the ultimate cause of irreproducibility and low magnetic shielding values<sup>19</sup> found for hafnium derivatives. Contamination by hydrogen is also frequently observed in  $\beta$ -ZrNCl and  $\beta$ -HfNCl, although lithium insertion and

superconductivity seem to be compatible with hydrogen contents up to 0.3 mol per formula. Cointercalation of hydrogen and oxygen in a  $\beta$ -MNCl matrix may be a possible source of inhomogeneities, as well as lithium insertion in excess of 0.5 mol/formula (full occupancy of the octahedral van der Waals voids), and both together may give rise to phase segregation. In light of all these facts, the optimization of the preparation process is crucial in view of understanding the origin of the different behavior of Zr and Hf derivatives, as well as the higher lithium uptake and critical temperature shown by the hafnium compound. Both facts deserve further investigation.

**Acknowledgment.** This study was supported by the CICYT (Grant MAT96-1037-C02), the Programa Sectorial de Promoción General del Conocimiento (Grants PB98-1424-CO2 and HF1998-43), the Picasso program from the Ministère de l'Éducation Nationale de la Recherche et de la Technologie (Grant 99102), and the Comissionat per Universitats i Recerca de la Generalitat de Catalunya (Grant 1998SGR00105).

CM991114G

(19) Fogg, A. M.; Green, V. M.; O'Hare, D. H. *J. Mater. Chem.* **1999**, *9*, 1547.